Development of Gallium Nitride Photoconductive Detectors

Dennis K. Wickenden, Zhenchun Huang, D. Brent Mott, and Peter K. Shu

Since 1994, the Applied Physics Laboratory has been collaborating with NASA Goddard Space Flight Center to develop photodetectors based on gallium nitride and aluminum gallium nitride material produced in the Milton S. Eisenhower Research and Technology Development Center. This article describes the results of our collaboration and highlights the development of gallium nitride photodetectors with responsivities and response times that are the best reported to date. These findings, obtained with simple structures, are of sufficient quality to launch the technology toward the development of practical devices with a variety of potential applications in future NASA missions.
(Keywords: Detector, Gallium nitride, Photoconductor, Ultraviolet.)

INTRODUCTION

Interest has always been high in the production and characterization of wide-bandgap semiconductor materials for a wide range of short-wavelength and high-temperature applications. Candidate material systems include silicon carbide (SiC), the Group II-VI semiconductors zinc sulfide (ZnS) and zinc selenide (ZnSe), and the Group IIIA nitrides. The hexagonal polytypes of SiC, although once considered excellent candidates for blue light-emitting diodes (LEDs) and more recently for high-temperature and high-power electronic devices, are not suitable for ultraviolet (UV) detector or emitter applications because of their indirect and comparatively low bandgaps ($E_g < 3.2$ eV).

Recent progress in developing blue–green LEDs and laser diodes in the ZnS_xSe_{1-x} alloy system[1] has been restricted to high-selenium alloys with bandgaps less than 2.8 eV. Higher-bandgap alloys continue to be plagued by autocompensation effects, whereby the introduction of a dopant atom is compensated by native defects and precludes well-behaved conductivity control. Thus, the Group IIIA nitrides are the preferred candidates for short-wavelength applications. Indium nitride (InN), gallium nitride (GaN), and aluminum nitride (AlN) have direct bandgaps of 2.0, 3.4, and 6.2 eV, respectively, with corresponding cutoff wavelengths of 620, 365, and 200 nm. Since they are miscible

with each other, these nitrides form complete series of indium gallium nitride ($In_{1-x}Ga_xN$) and aluminum gallium nitride ($Al_xGa_{1-x}N$) alloys, and it should be possible to develop detectors with wavelength cutoffs anywhere in this range.

Improvements in the growth and characteristics of gallium nitride[2] have resulted in significant inroads in device technology.[3] For example, high-efficiency blue-emitting metal insulator semiconductor LEDs[4] have been fabricated, and, with the advent of magnesium-doped *p*-type material, violet-emitting *pn*-junction LEDs[5] have been developed. Prototype GaN metal semiconductor field-effect transistors have also been reported.[6] In addition, high-quality, low-aluminum-content GaN/$Al_xGa_{1-x}N$ heterostructures have been produced that exhibit quantum confinement effects by photoluminescence,[7] stimulated emission under photon pumping,[8] and electron mobility enhancement.[9] Violet-emitting $In_{1-x}Ga_xN$/GaN LEDs with external quantum efficiencies of 0.22% have been made,[10] as have double-heterostructure blue- and green-emitting $In_{1-x}Ga_xN/Al_yGa_{1-y}N$ LEDs with external quantum efficiencies as high as 2.7%.[11] High-brightness blue, green, and yellow LEDs based on $Al_xGa_{1-x}N/In_{1-x}Ga_xN$ quantum well structures have recently been reported.[12] Finally, stimulated emission by current injection from an $Al_xGa_{1-x}N$/GaN/$In_{1-x}Ga_xN$ device has been observed.[13,14]

Along with this progress in light-emitting and microwave devices, a small but significant interest has grown in the development of photodetectors using the $Al_xGa_{1-x}N$ alloy system. Khan et al.[15] developed a metal–semiconductor–metal detector based on insulating GaN and obtained a responsivity of 2000 A/W (amperes of photocurrent per unit incident photon power) at 365 nm under an applied bias of 5 V. They recently reported an improved responsivity of 3000 A/W by employing an enhanced mobility GaN/$Al_xGa_{1-x}N$ heterostructure.[16] However, their detector performance varied from sample to sample, depending on the quality of the material. One main problem associated with GaN-based detectors has been their slow response times, originating from the high defect density of the starting material, which can also directly affect the stability and linearity of the devices.

Since 1994, APL has been collaborating with NASA Goddard Space Flight Center to develop photodetectors based on GaN and $Al_xGa_{1-x}N$ material produced in the Milton S. Eisenhower Research and Technology Development Center. We describe the results of this collaboration, in particular highlighting the development of GaN photodetectors.

PHOTOCONDUCTIVE DETECTORS

A semiconductor-based photoconductive detector can be viewed as a radiation-sensitive resistor,[17] as shown schematically in Fig. 1. In such a resistor, the current is generated by incoming photons that excite electrons from the valence to the conduction band and by at least some carriers being collected by one of the electrodes. Simply put, the photon-induced current I_{ph} is given by

$$I_{ph} = q\eta A\Phi g \ , \qquad (1)$$

where

- q = electronic charge,
- η = quantum efficiency (i.e., number of carriers generated per incident photon in the primary absorption process),
- A = device area exposed to incident radiation,
- Φ = incident flux, and
- g = photoconductive gain.

The two parameters influenced by the material characteristics are the quantum efficiency and the photoconductive gain.

In its simplest form, the photoconductive gain is given by

$$g = \frac{t}{t_t} \ , \qquad (2)$$

where t is the majority carrier's lifetime, and t_t is the transit time of the carrier between electrodes. This transit time can be approximated by

$$t_t = \frac{l^2}{m_e V_b} \ , \qquad (3)$$

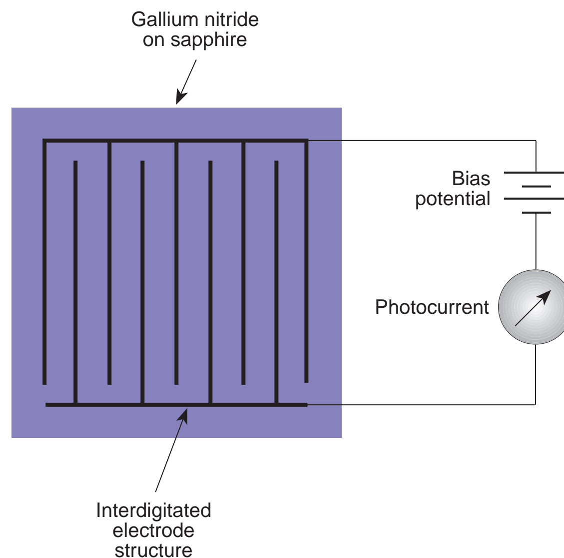

Figure 1. A diagram of a typical photoconductor circuit.

where l is the interelectrode spacing, m_e is the electron mobility, and V_b is the applied bias.

These equations all assume that the photons are absorbed uniformly throughout the photoconductor, that the sample thickness is small compared with the minority carrier's diffusion length, and that no surface or interface recombination of carriers occurs. Few, if any, of these assumptions are realized in practice. Therefore, photoconductor performance is usually reported by the catchall value of the overall responsivity, which is measured in terms of A/W. The incident power is the power falling over the total area of the device, including, sometimes, regions covered by the collection electrodes. The photon flux for a given incident power level is inversely proportional to the wavelength.

The photoconductive gain can be less than or greater than 1, depending on whether the drift length is greater than or less than the interelectrode spacing. A value greater than 1 implies that a free carrier has collected at one electrode and has immediately been replaced by the injection of an equivalent carrier at the opposite electrode. In effect, the free carrier continues to circulate until it is lost by either recombination or trapping.

The speed of response of the device is measured by the time it takes for the photogenerated signal to rise from 10 to 90% of the difference between the dark current and the steady-state current on exposure to the light (the so-called turn-on time, t_{on}) or the time it takes for the signal to fall from 90 to 10% of this value when the light is turned off (t_{off}). In general, these times are influenced by the presence of deep-level traps within the forbidden gap of the semiconductor. The exact influence of these traps is complicated, but a simple picture is as follows. In the dark, the trap is empty, but when the light is turned on, carriers used to fill the trap are lost to the collection process. The turn-on time is a function of both the concentration level of the trap (or traps) and the cross sections for filling them. When the light is turned off, the time for the current to fall to its dark current value is determined by the time it takes for the trap to empty.

From this discussion, we may conclude that the fabrication of a photoconductive device with superior characteristics requires the use of material with high quantum efficiency and high photoconductive gain to achieve large responsivity and high resistivity, which minimize the dark current and allow for high applied biases. In addition, low trap concentration is desirable to obtain fast response times. Of these, the only parameter intrinsic to any particular material is quantum efficiency, which is proportional to the absorption coefficient at photon energies near the bandgap. The other parameters are somewhat related and must be optimized during the material preparation stage, the device fabrication stage, or both.

DEVICE PROCESSING

Because of the unavailability of bulk GaN, single-crystal material is produced as epitaxial layers on foreign substrates by molecular beam epitaxy, vapor phase epitaxy, or metal organic chemical vapor deposition (MOCVD). APL has developed a technique using an Emcore GS3200 vertical spinning disc MOCVD reactor along with basal plane (00.1) oriented sapphire (α-Al_2O_3) substrates. Trimethylgallium (TMG), trimethylaluminum, and ammonia (NH_3) in a nitrogen (N_2) carrier gas are used as starting reagents. Before being loaded, the substrates are rigorously cleaned by an ultrasonic rinse in mild detergent, washed in 5:1:1 mixtures (by volume) of hot H_2O:HNO_3:H_2O_2 and H_2O:HCl:H_2O_2, rinsed in deionized H_2O, and finally dried with filtered N_2 gas. In addition, the substrates are heated *in situ* at 1023 K for 5 min before growth. Because α-Al_2O_3 has a significantly larger lattice parameter than GaN (0.476 nm compared with 0.319 nm), a low-temperature nucleation layer must be deposited prior to growth of the overlayer. This nucleation layer can be either AlN[18,19] or GaN.[20,21] The use of the latter was pioneered by APL.

For the photodetectors reported here, self-nucleation layers approximately 45 nm thick are deposited at 813 K (as measured with an optical pyrometer) using a TMG flow of 40 μmole/min, an NH_3 flow of 500 standard cm^3/min (sccm), and an N_2 flow of 4.0 standard L/min. The overlayers are grown at temperatures between 1300 and 1325 K using NH_3 flows in the range of 1000 to 2200 sccm; the N_2 flow was adjusted to maintain an approximately constant total gas input into the reactor. The substrates are rotated at 100 rpm to ensure uniform growth, and the process pressure was 70 Torr. Overlayer thicknesses are generally 1 to 2 μm.

Device development was undertaken at Goddard Space Flight Center. Because the sapphire substrate is electrically insulating, both electrodes had to be on the top GaN surface. In addition, because the minority carrier's lifetime is so short in direct-gap semiconductors, the electrodes are composed of pairs of interdigitated fingers. The patterning of these fingers is achieved by a conventional lift-off technique, wherein the wafer is thoroughly cleaned and a 500-nm-thick layer of photoresist is spun onto it. The interdigitated pattern is then photolithographically defined, and, when developed, the GaN surface on which the contact metal is required is exposed. The whole front surface is then covered, by vacuum evaporation, with a 20-nm layer of titanium and a 120-nm layer of aluminum. The wafer is then placed in a solvent and, as the unexposed photoresist is dissolved away, the unwanted metal layers are lifted off. Finally, the contacts are annealed at 318 K for 5 min in an N_2 atmosphere to ensure reliable ohmic characteristics. Upon completion of the fabrication

process the wafer is diced, and the individual devices are packaged and bonded for characterization without further passivation.

DEVICE RESULTS

The responsivity of a typical detector is shown as a function of incident wavelength in Fig. 2. Little response is seen at long wavelengths. Responsivity rises very sharply just below 370 nm, reaches a peak, and then falls off with decreasing wavelength. Also shown in Fig. 2 is the optical absorption spectrum of the epitaxial sample before device processing, scaled for comparison purposes. As expected, the sharp rise in responsivity corresponds to the energy gap of the GaN. The decrease in responsivity at short wavelengths due to the wavelength dependence of the optical flux is also indicated in the figure. The additional decrease can be attributed to many effects, including increased energy and hence shorter transit time of carriers, decreased penetration depth of incident photons, and increased surface recombination of carriers.

The effect of finger spacing in the range of 1 to 10 μm on responsivity is shown in Fig. 3. In these samples the finger width was constant at 1 μm, and the responsivities were corrected for the exposed area. The black curve gives a power dependence of –2.5, compared with the expected 2 from Eq. 3. The difference, together with the deviation from the power law at small spacings, can be attributed to the oversimplification of the theory in that surface recombination will be an important factor in carrier loss on these unpassivated surfaces. The figure does, however, clearly demonstrate that, as expected, responsivity is a strong function of interelectrode spacing, and the smaller the spacing, the better the responsivity.

To examine the effect of growth conditions on device properties, we conducted a study to determine the ratio of NH_3 to TMG in the growth of the overlayer,

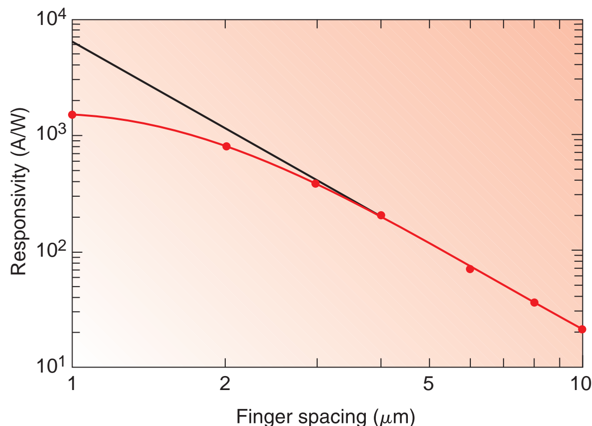

Figure 3. Effect of interdigitated finger spacing on responsivity (red curve). The black curve represents a power dependence of –2.5.

since this parameter should significantly affect GaN stoichiometry and crystal perfection. The device geometry consisted of 14 interdigitated fingers on each contact, with each finger 4 μm wide and a nominal finger separation of 4 μm. The detectors were operated with a bias voltage of 10 V.

The responsivity and response times as functions of NH_3 flow rate are given in Figs. 4 and 5, respectively, which show that responsivity increases almost linearly with NH_3 flow rate and response times decrease monotonically. In fact, the responsivity (3200 A/W), turn-on time (0.3 ms), and turn-off time (0.6 ms) of the sample prepared with an NH_3 flow rate of 2200 sccm are the best values reported to date for GaN photoconductors. The resistivity of the material increases approximately exponentially with NH_3 flow rate from 4×10^7 Ω·cm at 1000 sccm to 3×10^9 Ω·cm at 2200 sccm. This large resistivity resulted in a dark current of only 5 pA for the best detector.

Figure 6 illustrates the frequency dependence of the signal level of devices made from material produced

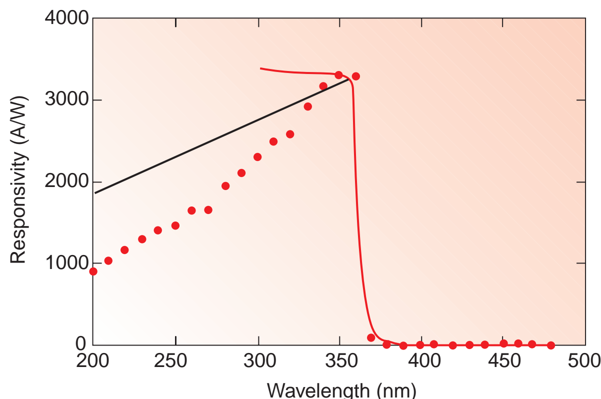

Figure 2. Responsivity as a function of incident wavelength (red dots). The red curve gives the optical absorption. The black curve represents the dependence of flux on wavelength.

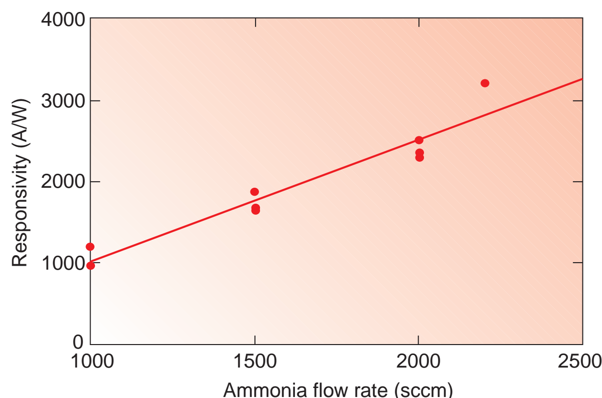

Figure 4. Responsivity as a function of NH_3 flow rate (sccm = standard cm^3/min).

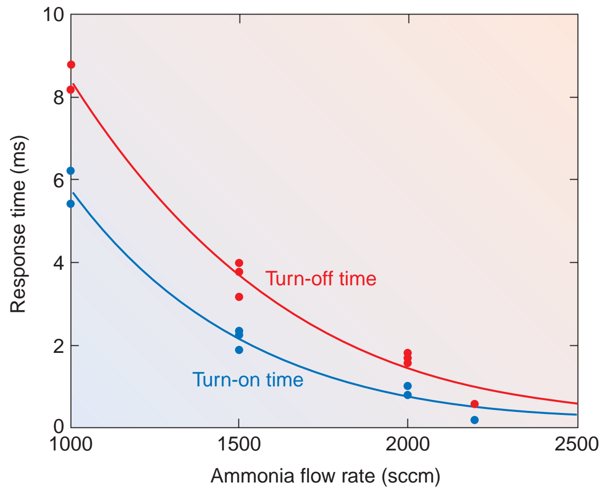

Figure 5. Turn-on and turn-off time as a function of NH_3 flow rate.

using the different NH_3 flow rates. It also shows that the most stable devices are produced from material with the highest NH_3 flow rate, whereas material grown under a low NH_3 flow rate produces devices with poor stability, particularly in the low-frequency region.

To understand more fully the effect of the NH_3 flow rate on material properties, deep-level characteristics were studied by thermally stimulated current (TSC) and photocurrent spectroscopies. In the former technique, the interdigitated sample is cooled to a low temperature (30 K) and irradiated with above-bandgap UV light. The photogenerated carriers fill all the available trap levels. The sample is then heated at a constant rate in the dark, and the current generated as the various traps are emptied is measured. The resultant trace consists of a series of peaks, which correspond to individual trap levels whose activation energy (E_a) can be obtained from the approximation[22]

$$E_a = kT_m \ln(T_m^4 / b) , \quad (4)$$

where k is the Boltzman constant, T_m is the peak temperature, and b is the heating rate.

Similarly, the concentration of each trap can be obtained from the approximation[23]

$$Q = AqN_T L^* , \quad (5)$$

where Q is the total charge, which is equal to the area under the TSC peak, N_T is the trap concentration, and L^* is the effective drift distance of carriers under applied bias. We assume that all the carriers being emptied from the traps are collected by electrodes and that they contribute to the TSC current. In this case, we take L^* to be 1 μm (the spacing between the electrodes in the test samples). The actual trap concentration may be lower than the calculated one; however, the relative trap concentrations should not affect the comparison of results. The TSC technique can only detect deep levels in the range of 0 to 0.75 eV below the conduction band or above the valence band.

The photocurrent technique is used to measure deeper levels. The sample is held under bias and illuminated with monochromatic light from the infrared to the UV. Any carriers trapped in deep levels are released and collected, since the energy of the incident photons corresponds to that of the deep level.

A typical TSC spectrum, obtained with a 20-V bias, is shown in Fig. 7. Also shown is the dark current, which was obtained under the same condition but without the illumination at low temperature. Five levels, T1–T5, are observed in a temperature range of 40 to 360 K, with activation energies of 0.11, 0.24, 0.36, 0.53, and 0.62 eV, respectively. We noted in some samples that the 0.11-eV level (T1) had a high concentration in the first temperature scan, was eliminated after the second run, and never reappeared in subsequent runs. We inferred from this behavior that the T1 level must be related to surface states present in the

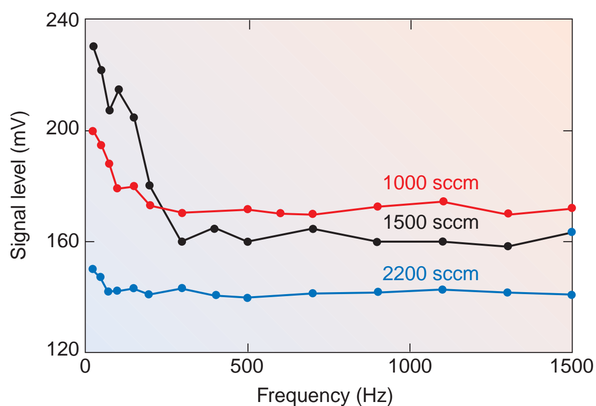

Figure 6. Signal level of samples produced with different NH_3 flow rates as a function of frequency.

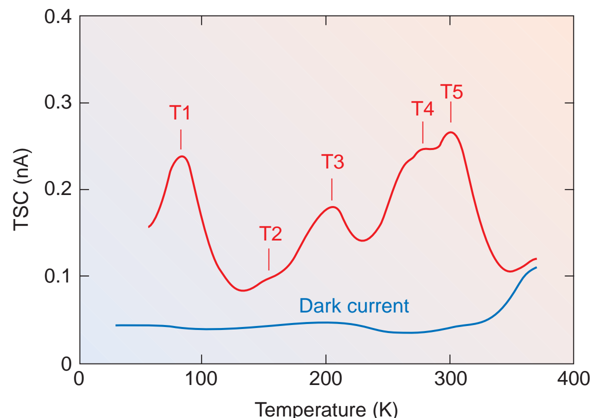

Figure 7. Typical thermally stimulated current (TSC) spectrum obtained with a 20-V bias. (Levels T1–T5 correspond to activation energies of 0.11, 0.24, 0.36, 0.53, and 0.62 eV, respectively.)

samples caused by moisture or a native oxide and that it is not associated with a bulk defect. The 0.62-eV level (T5) had the highest concentration among all the observed traps. The dark current measurement showed that this level dominated the conduction in the high-temperature range (>300 K). The T5 concentration as a function of NH_3 flow rate is given in Fig. 8, where it decreases dramatically with increasing NH_3 flow until, at 2200 sccm, it reaches the minimum detection limit of the measurement system.

A typical photocurrent spectrum normalized using a calibrated light source is illustrated in Fig. 9. In addition to the peak corresponding to the bandgap at about 3.41 eV, three other deep levels, D1, D2, and D3, were observed in this material at energy levels of 2.36, 1.70, and 1.32 eV, respectively.

We also studied the effect of furnace annealing on the deep-level behavior. This was done at 1273 K under an N_2 environment without proximity capping. Before contact fabrication, the annealed wafer was dipped into an NaOH (40%) solution for 5 min to remove any possible surface damage. The T5 level was the only one left after this treatment; levels T2, T3, and T4 disappeared. An increase in the dark current after annealing was also observed, indicating that the GaN became more conducting. In contrast, no significant change was seen in the photocurrent spectra or the relative peak intensities of the three D levels after annealing. The T5 concentration increased approximately exponentially with annealing time, as shown in Fig. 10.

We appear to have correlated the improvement in responsivity and response times of GaN photoconductors with increasing NH_3 flow rate with the concomitant decrease in deep levels in the material. In particular, T5, which is located 0.62 eV below the conduction band and attributed to either gallium antisites or nitrogen vacancy–related complexes, was found to be common and dominant in all GaN material grown with the different NH_3 flow rates. However, the concentration of this trap decreased significantly with increasing NH_3 flow rate, as shown in Fig. 8. The other traps observed did not exhibit such flow dependence. This probable correlation is not too surprising since the increase in NH_3 flow rate, and hence the nitrogen–gallium ratio, should decrease the concentration of either gallium antisites or nitrogen vacancy–related defects in the material.

Similarly, since GaN evaporates incongruently at high temperatures, the annealing procedure should cause an increase in such stoichiometric defects. However, other factors may affect the performance of the GaN photoconductor detectors. For example, the mobility or minority carrier lifetime may also be improved in material grown with increased NH_3 flow rate. Further work is under way to clarify this point. Of the other deep levels detected, the 0.53-eV level (T4) reported here is near the 0.49-eV level observed by others in Si-doped[24] and undoped GaN.[25] This level becomes dominant in Si-doped and Si-implanted layers, and is probably associated with Si-related defects.

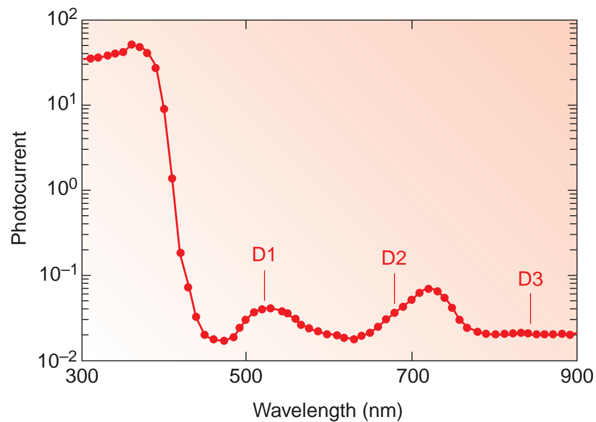

Figure 9. Typical photoconductivity spectrum, given in arbitrary units, obtained with a 20-V bias. Deep levels D1–D3 correspond to energy levels of 2.36, 1.70, and 1.32 eV, respectively.

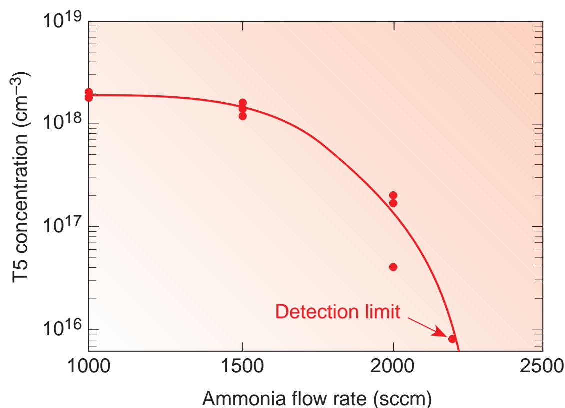

Figure 8. Level T5 concentration as a function of NH_3 flow rate.

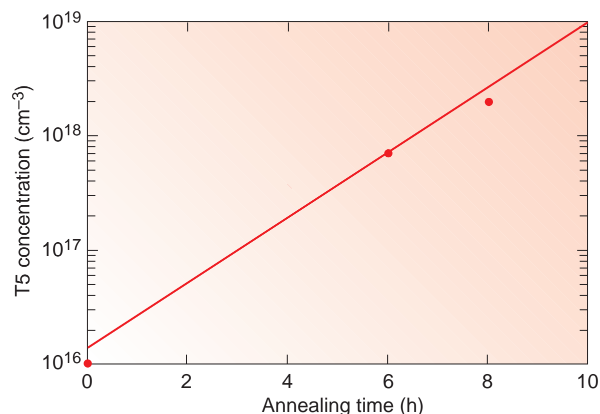

Figure 10. Level T5 concentration as a function of annealing time at 1273 K.

To date, we have no identification for levels T2 and T3 detected by TSC or levels associated with D1–D3 detected by photocurrent measurements. However, they all seem to be less important than level T5 for optimizing device performance.

In summary, we have developed a materials growth capability as well as a device processing capability that results in GaN photoconductors with responsivities and response times that are the best values reported to date for this class of device. Work is proceeding to further develop these prototypes into devices capable of meeting a variety of potential applications of interest to NASA.

POTENTIAL APPLICATIONS

NASA's interest in GaN photodetectors is in their potential to provide enhanced-performance or lower-cost scientific instruments for future missions. Today's UV instruments chiefly use photomultiplier tubes (PMTs), microchannel plates (MCPs), or silicon charge-coupled devices (CCDs). The most significant shortcomings of PMTs and MCPs with respect to instrument costs are their mass, volume, and power requirements. These detectors are complex assemblies, making them much larger and heavier than a corresponding focal plane device. The required operating bias (commonly 3500–5000 V for an MCP) must come from high-voltage power supplies that add significant mass and volume to an instrument in addition to power demands on the spacecraft. The detectors are also susceptible to damage or destruction by high-voltage arcing. GaN detectors are typically run at zero bias for photodiodes or at a low bias (typically 5 V) for photoconductors, eliminating the need for high-voltage power supplies and the danger of destruction by arcing.

Silicon CCDs have lower mass and volume, require less voltage to operate, and are more environmentally rugged than PMTs and MCPs. However, because of its smaller bandgap energy (1.1 eV), silicon is sensitive to photons throughout the visible spectrum and into the infrared. This is a disadvantage to most Earth and space science instruments since the UV signal to be observed is commonly accompanied by a stronger signal in the visible or infrared that must be suppressed. With their larger bandgaps, materials such as GaN, SiC, and diamond have long-wavelength cutoffs at shorter wavelengths than silicon. With a long-wavelength cutoff of 365 nm, GaN neatly divides the UV from the visible. If silicon-based detectors are used for UV observations in the presence of visible or near-infrared radiation, expensive blocking filters and extensive stray light baffling must be used to reject the unwanted signal.

In the near term, GaN-based detectors will most likely find application in Earth-observing instruments. NASA is searching for low-cost technologies to meet programmatic objectives for global environmental observations. There is a particular need for mapping and sounding instruments that can measure a variety of environmental and climatic parameters (e.g., ozone, water vapor, sulfur dioxide, temperature, aerosols, incident UVB radiation). Such low-cost, high-quality spaceborne instruments are possible with emerging technologies such as GaN-based UV detectors. These detectors are uniquely applicable for UV remote sensing since they can, as demonstrated in the previous discussion, have high responsivity in the UV but little in the visible. This attribute enormously simplifies the instrument's optical systems, which are often driven by the need to reject visible light and eliminate stray light.

For space science applications, the advantages of the current technology will keep it from being superseded in the near future. Even with their inherent liabilities, MCPs and silicon CCDs will likely be the appropriate choice because of their maturity and their availability as large-area arrays. GaN and the other wide-bandgap–based detectors are available as individual elements, linear arrays, and small-area arrays of either photoconductors or photodiodes. The development of CCDs or large-bandgap photodiode arrays will require a significant advance over today's technology.

REFERENCES

[1] Gunshor, R. L., and Nurmikko, A. V., "The First Compact Blue/Green Diode Lasers: Wide-Bandgap II-VI Lasers Come of Age," *Proc. IEEE* **82**, 1503–1513 (1994).

[2] Wickenden, D. K., Bryden, W. A., Kistenmacher, T. J., Bythrow, P. F., and Strohbehn, K., "Development of $Al_xGa_{1-x}N$ Alloy Semiconductors for Solar-Blind Ultraviolet Seeker Applications," *Johns Hopkins APL Tech. Dig.* **16**(3), 246–257 (1995).

[3] Strite, S., and Morkoç, H., "GaN, AlN, and InN: A Review," *J. Vac. Sci. Technol. B* **10**, 1237–1266 (1992).

[4] Akasaki, I., Amano, H., Hiramatsu, K., and Sawaki, N., "High Efficiency Blue LED Utilizing GaN Film with AlN Buffer Layer Grown by MOVPE," *Inst. Phys. Conf. Ser.* **91**, 633–636 (1988).

[5] Amano, H., Kito, H., Hiramatsu, K., and Akasaki, I., "P-Type Conduction in Mg-Doped GaN Treated with Low-Energy Electron Beam Irradiation (LEEBI)," *Jpn. J. Appl. Phys.* **28**, L2112–2114 (1989).

[6] Khan, M. A., Kuznia, J. N., Bhattarai, A. R., and Olson, D. T., "Metal-Semiconductor Field Effect Transistor Based on Single Crystal GaN," *Appl. Phys. Lett.* **62**, 1786–1787 (1993).

[7] Itoh, K., Kawamoto, T., Amano, H., Hiramatsu, K., and Akasaki, I., "Metalorganic Vapor Phase Epitaxial Growth and Properties of GaN/$Al_{0.1}Ga_{0.9}N$ Layered Structures," *Jpn. J. Appl. Phys.* **30**, 1924–1927 (1991).

[8] Amano, H., Asahi, T., Kito, M., and Akasaki, I., "Stimulated Emission in MOVPE-Grown GaN Film," *J. Luminescence* **48/49**, 889–892 (1991).

[9] Khan, M. A., Van Hove, J. M., Kuznia, J. N., and Olson, D. T., "High Electron Mobility GaN/$Al_xGa_{1-x}N$ Heterostructures Grown by Low-Pressure Metalorganic Chemical Vapor Deposition," *Appl. Phys. Lett.* **58**, 2408–2410 (1991).

[10] Nakamura, S., Senoh, M., and Mukai, T., "High-Power InGaN/GaN Double Heterostructure Violet Light Emitting Diodes," *Appl. Phys. Lett.* **62**, 2390–2392 (1993).

[11] Nakamura, S., Mukai, T., and Senoh, M., "High-Brightness InGaN/AlGaN Double-Heterostructure Blue–Green Light-Emitting Diodes," *J. Appl. Phys.* **76**, 8189–8191 (1994).

[12] Nakamura, S., Senoh, M., Iwasa, N., and Nagahama, S., "High-Brightness InGaN Blue, Green and Yellow Light-Emitting Diodes with Quantum Well Structures," *Jpn. J. Appl. Phys.* **34**, L797–L799 (1995).

[13] Akasaki, I., Amano, H., Sota, S., Sakai, H., Tanaka, T., and Koike, M., "Stimulated Emission by Current Injection from an AlGaN/GaN/GaInN Quantum Well," *Jpn. J. Appl. Phys.* **34**, L1517–L1519 (1995).

[14] Nakamura, S., Senoh, M., Nagahama, S., Iwasa, N., Yamada, T., Matsushita, T., Kiyoku, H., and Sugimoto, Y., "InGaN-based Multi-Quantum-Well-Structure Laser Diodes," *Jpn. J. Appl. Phys.* **35**, L74–L76 (1996).

[15] Khan, M. A., Kuznia, J. N., Olson, D. T., Van Hove, J. M., Blasingame, M., and Reitz, L. F., "High-Responsivity Photoconductive Ultraviolet Sensors Based on Insulating Single-Crystal GaN Epilayers," *Appl. Phys. Lett.* **60**, 2917–2919 (1992).

[16] Khan, M. A., Shur, M. S., Chen, Q., Kuznia, J. N., and Sun, C. J., "Gated Photodetector Based on GaN/AlGaN Heterostructure Field Effect Transistor," *Electronics Lett.* **31**, 398–400 (1995).

[17] Razeghi, M., and Rogalski, A., "Semiconductor Ultraviolet Detectors," *J. Appl. Phys.* **79**, 7433–7472 (1996).

[18] Yoshida, S., Misawa, S., and Gonda, S., "Improvements on the Electrical and Luminescent Properties of Reactive Molecular Beam Epitaxially Grown GaN Films Using AlN-Coated Sapphire Substrates," *Appl. Phys. Lett.* **42**, 427–429 (1983).

[19] Amano, H., Sawaki, N., Akasaki, I., and Toyoda, Y., "Metalorganic Vapor Phase Epitaxial Growth of a High Quality GaN Film Using an AlN Buffer Layer," *Appl. Phys. Lett.* **48**, 353–355 (1986).

[20] Wickenden, D. K., Kistenmacher, T. J., Bryden, W. A., Morgan, J. S., and Wickenden, A. E., "The Effect of Self-Nucleation Layers on the MOCVD Growth of Gallium Nitride on Sapphire," *Mat. Res. Soc. Symp. Proc.* **221**, 167–172 (1991).

[21] Nakamura, S., "GaN Growth Using a GaN Buffer Layer," *Jpn. J. Appl. Phys.* **30**, L1705–L1707 (1991).

[22] Huang, Z. C., Xie, K., and Wie, C. R., "A Simple and Reliable Method of Thermoelectric Effect Spectroscopy for Semi-Insulating III-V Semiconductors," *Rev. Sci. Instrum.* **62**, 1951–1954 (1991).

[23] Xie, K., Huang, Z. C., and Wie, C. R., "Deep Level Studies in MBE GaAs Grown at Low Temperature," *J. Electron. Mater.* **20**, 553 (1991).

[24] Götz, W., Johnson, N. M., Amano, H., and Akasaki, I., "Deep Level Defects in *n*-Type GaN," *Appl. Phys. Lett.* **65**, 463–465 (1994).

[25] Lee, W. I., Huang, T. C., Guo, J. D., and Feng, M. S., "Effects of Column III Alkyl Sources on Deep Levels in GaN Grown by Organometallic Vapor Phase Epitaxy," *Appl. Phys. Lett.* **67**, 1721–1723 (1995).

THE AUTHORS

DENNIS K. WICKENDEN is a physicist in the Sensor Science Group of the Milton S. Eisenhower Research and Technology Development Center at APL. He received B.Sc. and Ph.D. degrees from the Imperial College of Science and Technology (University of London) in 1962 and 1965, respectively. He was elected a Fellow of the Institute of Physics in 1973. After a postdoctoral fellowship at the University of Notre Dame, Dr. Wickenden worked at the GEC Hirst Research Centre in England on the growth, characterization, and application of a variety of compound semiconductors. In 1985, he became a senior scientist at Crystal Specialties, Portland, Oregon, where he developed epitaxial growth equipment for the semiconductor industry. Dr. Wickenden joined APL in 1987 as a Senior Staff Physicist. His current research interests include growth and characterization of gallium nitride and related alloys and the development of microelectromechanical sensors. His e-mail address is Dennis.Wickenden@jhuapl.edu.

ZHENCHUN HUANG is a principal scientist at Hughes STX Corporation, working at the NASA Goddard Space Flight Center. He received B.Sc. and M.Sc. degrees in physics from Nanjing University, China, in 1984 and 1987, respectively, and a Ph.D. degree in electrical engineering from the State University of New York at Buffalo in 1993. Before joining Hughes STX in 1995, he studied semiconductor material growth and characterization at the University of Maryland, Baltimore County, as a postdoctoral fellow. Dr. Huang's research interests include characterization of gallium nitride and related alloys and their application to ultraviolet detector arrays. He has published more than 40 journal papers. His e-mail address is ted@ipx-18.gsfc.nasa.gov.

D. BRENT MOTT is an engineer in the Solid State Device Development Branch at the NASA Goddard Space Flight Center. He received a B.S. degree in physics from the University of Maryland in 1981. After graduation he spent several years building far-infrared spectrometers for astronomical observations at Goddard's Infrared Astrophysics Branch. Having obtained a fellowship from Martin Marietta, Mr. Mott received an M.S. degree in electrical engineering. He then returned to NASA's Solid Stated Device Development Branch, working primarily on the micromachined silicon X-ray calorimeters and infrared bolometers. He is currently leader of the Device Development Group. His e-mail address is Brent.Mott@gsfc.nasa.gov.

PETER K. SHU is the head of the Solid State Device Development Branch at the NASA Goddard Space Flight Center. He received a B.S. degree in 1973, and an M.S. degree in electrical engineering from the University of Michigan, Ann Arbor, in 1975. Mr. Shu has been involved in scientific infrared instrument development since 1982. He was on the Infrared Array Camera proposal team for the Space Infrared Telescope Facility and has been selected as a co-investigator for that effort. He has served as systems engineer for the Broad Band X-Ray Telescope Project and as focal plane engineer for the Composite Infrared Spectrometer on the Cassini mission. His e-mail address is pks718@www710. gsfc.nasa.gov.